ChemistryEurope

ChemistryEurope
Excellence in Chemistry Research Worldwide

RESEARCH ARTICLE OPEN ACCESS

UPO-Mimetic Engineering of CYP199A4 Enables Enhanced Peroxygenase Activity via the Hydrogen Peroxide Shunt Pathway

Pablo Velázquez García | Thomas Hilberath | Peter-Leon Hagedoorn | Frank Hollmann

Department of Biotechnology, Delft University of Technology, Delft, The Netherlands

Correspondence: Peter-Leon Hagedoorn (p.l.hagedoorn@tudelft.nl) | Frank Hollmann (f.hollmann@tudelft.nl)

Received: 14 November 2025 | **Revised:** 26 January 2026 | **Accepted:** 4 February 2026

Keywords: enzyme mechanism | H_2O_2 | monooxygenase | oxyfunctionalization | peroxygenases

ABSTRACT

Engineering an acid–base dyad into the peroxygenase-enabled mutant CYP199A4^{T252E} yielded four in silico-designed double mutants, of which CYP199A4$^{F182R/T252E}$ showed the best dyad-like geometry and was characterized further. It delivered ~10-fold higher initial H_2O_2-driven O-demethylation activity than wild type and CYP199A4^{T252E}, alongside reduced catalase activity and improved peroxide utilization. However, it was more prone to H_2O_2-induced heme bleaching and rapid inactivation under standard dosing; slow, controlled H_2O_2 feeding sustained catalysis for hours. Overall, adding a second basic residue boosts per-oxy-gen-ase-like activity but reduces oxidative robustness, underscoring the trade-off between efficiency and peroxide tolerance and guiding future engineering of robust P450 peroxygenases.

1 | Introduction

Cytochrome P450 enzymes (P450s) constitute a large and diverse superfamily of heme-containing monooxygenases found across all domains of life, including bacteria, fungi, plants, and animals, where they play a crucial role in metabolism. P450s catalyze oxyfunctionalisation reactions incorporating one atom of molecular oxygen into (non) activated C—H- and C=C-bonds [1]. They exhibit a wide range of substrate specificities, from very narrow (e.g. P450s involved in steroid biosynthesis in mammals or secondary metabolite production in plants) to very broad, as seen for example for microsomal P450s involved in xenobiotic detoxification [2].

A defining characteristic of P450 enzymes is their often high regio- and stereoselectivity, features usually unachievable through conventional chemical methods. This makes them highly attractive for applications in biocatalysis and pharmaceutical syntheses. However, several challenges must be addressed before their widespread implementation. These include their reliance on complex electron transfer chains and costly cofactors, together with the so-called oxygen dilemma [3], referring to the uncoupling of reducing equivalents into side reactions resulting from the use of O_2 as the oxygen source.

The catalytic cycle of a P450 enzyme (Scheme 1) [4] involves the reductive activation of molecular oxygen and insertion of one oxygen atom into a substrate. It begins with substrate binding close to the ferric heme iron (Fe^{3+}), expelling a bound water molecule (associated with a low spin to high spin shift) which increases the redox potential and allows for the first electron transfer, reducing the iron to Fe^{2+}. Molecular oxygen then binds to form a ferrous–dioxygen complex. A second electron reduces this to a peroxo intermediate, which undergoes protonation to form a hydroperoxo species. Further protonation cleaves the O—O bond, releasing water and generating a highly reactive oxoferryl species (Fe^{4+}=O), known as Compound I. This intermediate abstracts a hydrogen atom from the substrate, forming a substrate radical and Fe^{3+}—OH, followed by "oxygen rebound" to produce the hydroxylated product. The product is released, and the enzyme returns to its resting Fe^{3+} state, ready for another catalytic cycle.

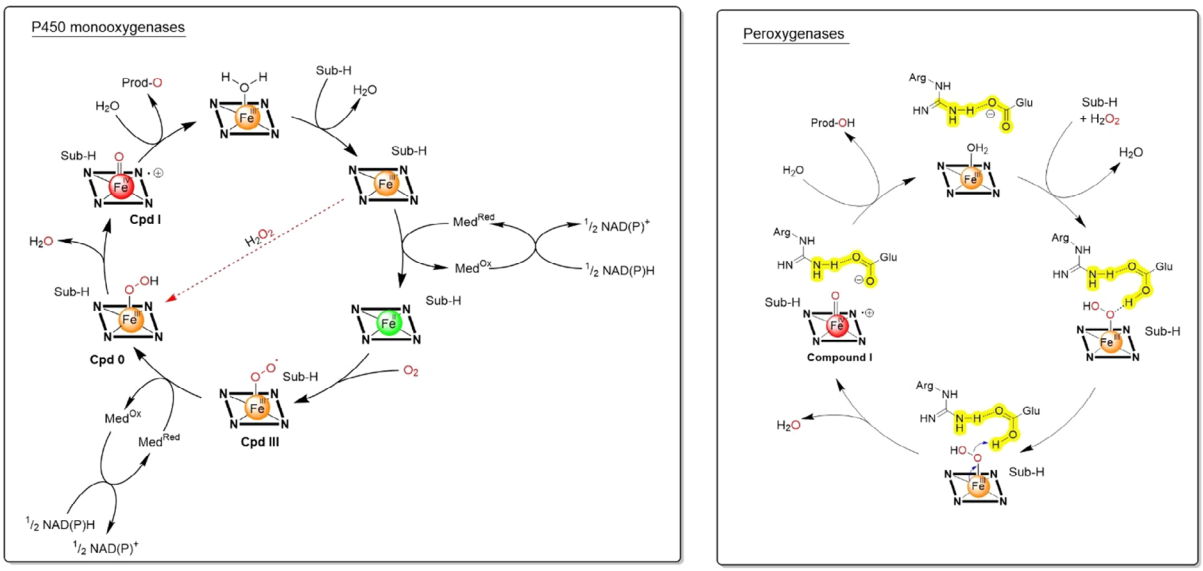

SCHEME 1 | Comparison of P450 monooxygenases and peroxygenases**.** In both cases, a highly oxidized oxyferryl iron species (Compound I) serves as the oxyfunctionalisation agent. In P450 monooxygenases, molecular oxygen is reduced in two successive single-electron transfer steps via mediators (typically ferredoxins or flavodoxins), thereby generating Compound I. In peroxygenases, Compound I is formed directly from pre-reduced H_2O_2, thus bypassing the electron transfer steps. The catalytically relevant Glu/Arg-dyad is highlighted.

Phylogenetic analyses suggest that P450-like enzymes evolved from a common ancestor more than 3.3 billion years ago [5], long before Earth's atmosphere became oxygen-rich. These early P450 enzymes were likely involved in peroxide-driven reactions and only later acquired their modernmonooxygenase function as described above. The "peroxygenase-first" hypothesis also implies that modern P450 monooxygenases could be re-engineered to function as peroxygenases. Beyond the conceptual appeal of this

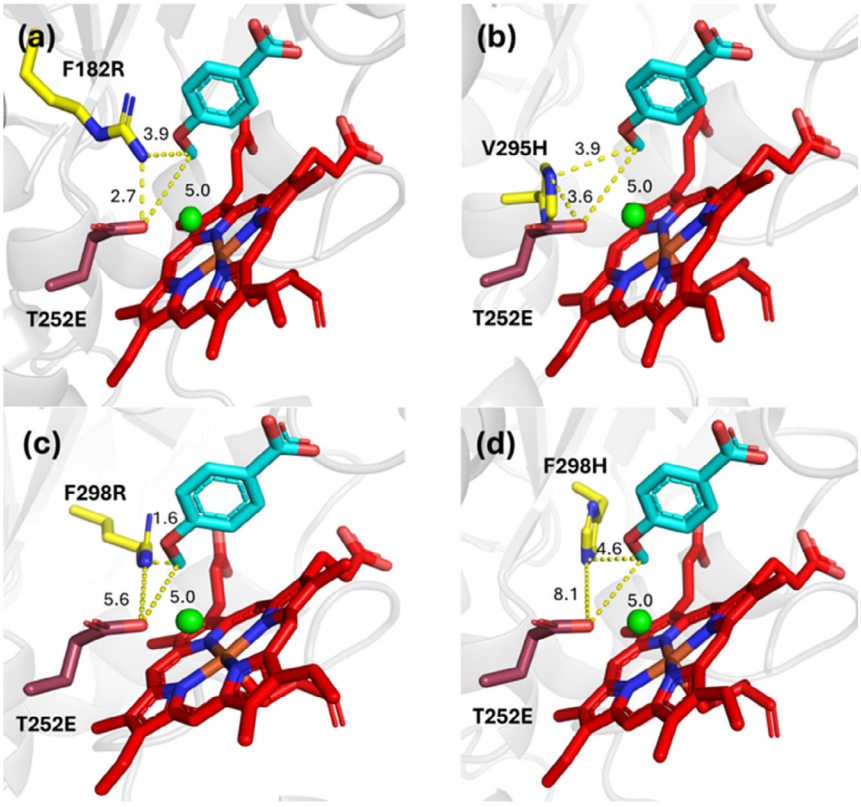

FIGURE 1 | Proposed mutations aiming for the improvement of peroxygenase activity of CYP199A4^{T252E}. The heme is visible red, 252E residue in dark red, the substrate in cyan, mutant residues in yellow, and the water molecule in green. (a) CYP199A4$^{F182R/T252E}$, (b) CYP199A4$^{T252E/V295H}$, (c) CYP199A4$^{T252E/F298R}$, (d) CYP199A4$^{T252E/F298H}$.

reverse evolutionary approach, it also offers practical advantages, such as highly simplified reaction schemes. Instead of relying on reductive activation of O_2, peroxygenases utilize already reduced O_2 in the form of H_2O_2 (or organic hydroperoxides). Hence, the catalytic competent Compound I is formed directly from the resting state in a sequence of H_2O_2-binding to the Fe^{3+}-centre, de- and reprotonation followed by water elimination (Scheme 1).

One major structural difference between peroxygenases and P450 monooxygenases is the absence of a catalytic base in the active site of the latter, such as a histidine or glutamate residue (Scheme 1) [6]. This observation has inspired researchers to explore H_2O_2-driven catalysis by P450 monooxygenases through the introduction of catalytic bases, either genetically [7–10], or via so-called decoy molecules [11–14]. Bell and coworkers, for example, have demonstrated that a single amino acid exchange (T252E) within the CYP199A4 from *Rhodopseudomonas palustris* HaA2 significantly increased its peroxygenase activity [10].

However, what these studies have so far largely overlooked is the fact that particularly active peroxygenases, such as *Aae*UPO from *Agrocybe aegerita* [15–19], possess a second base in their active site. This observation has led us to hypothesize that a catalytic dyad may play a crucial role in the H_2O_2-activation. Thus, we decided to screen the catalytic pocket of the CYP199A4^{T252E} for potential amino acids that, when mutated to basic residues, would further increase the peroxygenase activity of said variants.

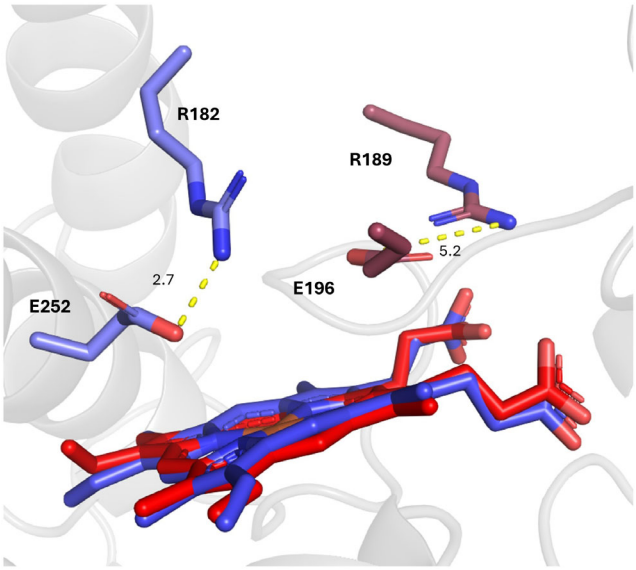

FIGURE 2 | Alignment of the heme and the natural acid–base pair in *Aae*UPO (**red**) and the heme and one of the designed acid–base pair in CYP199A4 (**blue**).

2 | Results and Discussion

2.1 | In Silico Design and Minimal Energy Simulations of CYP199A4 T252E Variants

To test our hypothesis, we used the T252E mutant of CYP199A4, previously reported by Bell and coworkers (PDB: 7REH), as a starting point for generating further variants. The selection of potential mutants was guided by three criteria: first, the amino acid substitution should introduce an additional basic residue, such as arginine or histidine; second, the substituted residue should be located in close proximity to the heme; and third, the mutation should minimally affect the positioning of the substrate and other active site residues. Using this approach, we identified several promising double mutants: CYP199A4$^{\mathbf{F182R}/T252E}$ (Figure 1a), CYP199A4$^{T252E/\mathbf{V295H}}$ (Figure 1b), CYP199A4$^{T252E/\mathbf{F298H}}$ (Figure 1c), and CYP199A4$^{T252E/\mathbf{F298R}}$ (Figure 1d). These variants are considered promising because the newly introduced basic residue (H or R) adopts a favorable orientation toward the heme and is positioned in close proximity to the previously introduced glutamate (T252E), potentially enabling formation of the proposed catalytic dyad. It should also be noted that, so far, we have been unable to generate the mutant CYP199A4$^{\mathbf{F182H}/T252E}$.

YASARA [20] simulations (Figure S2) indicated that the proposed additional mutations would not significantly affect the orientation of the model substrate relative to the heme. In particular, the CYP199A4$^{F182R/T252E}$ mutant exhibited a remarkable

(a)

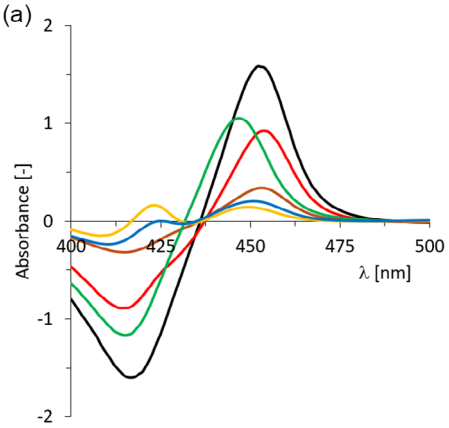

(b)

CYP199A4 variant	Total protein concentration [g L^{-1}][a]	c(P450) [μM][b]	Total P450 [nmol][c]
WT	3.54	17.40	304.50
T252E	3.12	10.19	305.56
F182R/T252E	3.72	11.53	317.05
T252E/V295H	2.53	3.73	121.20
T252E/F298R	3.65	1.60	43.93
T252E/F298H	3.74	2.23	66.84

FIGURE 3 | CO-difference spectra (a) and yields of CYP199A4 variants in the total volume of crude extract of 200 mL cultures of recombinant *E. coli* C43(DE3) (b). Total protein concentration measured by BSA assay [a], concentration as determined via CO-difference spectra [b], and total amount [c] of CYP199A4 variants obtained by CO-difference spectra.

similarity to the acid–base pairs commonly observed in long unspecific peroxygenases (Figure 2) [21].

2.2 | Production and Biochemical Characterization of CYP199A4 Variants

The double mutants described above were generated from CYP199A4^{T252E} by site-directed mutagenesis and recombinantly expressed in *E. coli*. For comparison, wild-type CYP199A4 and the parent CYP199A4^{T252E} mutant were also expressed. According to SDS-PAGE analysis the mutants CYP199A4$^{F182R/T252E}$, and CYP199A4$^{T252E/F298H}$ were expressed at comparable levels to CYP199A4^{wt} and CYP199A4^{T252E}, whereas the expression levels of CYP199A4$^{T252E/V295H}$ and CYP199A4$^{T252E/F298R}$ were somewhat lower (Figure S3).

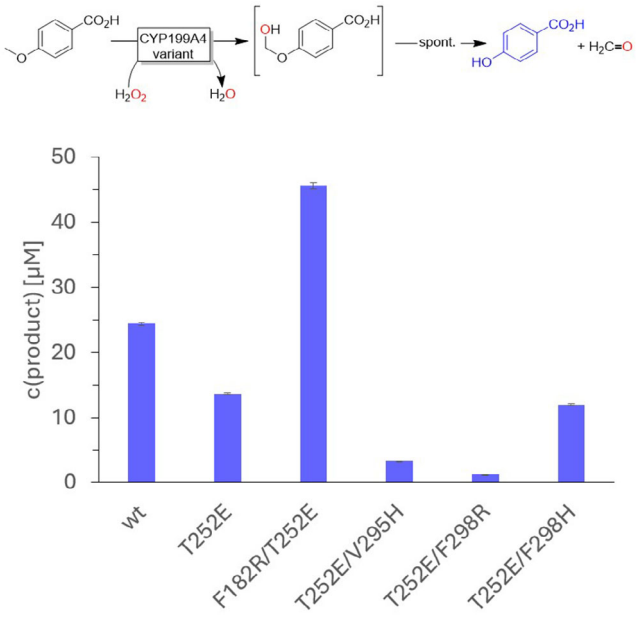

FIGURE 4 | Evaluation of the peroxygenase activity of CYP194A4 variants in crude extracts. Reaction conditions: 50 mM KPi buffer (2 vol% ACN), pH 7.5, total volume 0.5 mL (in horizontal shaker, 600 rpm), $T = 30°C$, $t = 3.5$ h; c(CYP199A4) = 2.5 µM enzyme (crude extract) c(4-methoxybenzoic acid) = 1 mM, $c(H_2O_2)_{final}$ = 25 mM (added in two steps at $t = 0$ and $t = 105$ min). Values have been corrected for background (empty vector) and represent the average of duplicates. Product concentrations were deduced from calibration curves recorded under similar reaction conditions.

To estimate the concentration of active enzyme variants, CO-difference spectra were recorded for all crude extracts (Figure 3).

The UV–vis spectra of the various enzyme variants demonstrate that the highest concentration of active enzyme was achieved for CYP199A4^{wt}, followed by the double mutant CYP199A4$^{F182R/T252E}$ and then the single mutant CYP199A4^{T252E}. Most of the remaining mutants displayed lower concentrations and/or reduced stability in crude extracts. This decreased stability is evident from the appearance of a spectral shoulder around 420 nm, indicating that a fraction of the cytochrome P450 enzyme had lost its cysteinyl ligation upon dithionite reduction and exposure to carbon monoxide, rendering it inactive [22]. Interestingly, CYP199A4$^{F182R/T252E}$ not only exhibited slightly improved expression compared to CYP199A4^{T252E}, but also demonstrated a blueshifted Soret peak for the ferrous CO-bound enzyme (452 to 446 nm). This shift is most likely due to a subtle alteration in the orientation of the heme caused by the arginine mutation positioned directly above it (Figure S2). Similar effects resulting from single or multiple mutations have previously been reported for various P450 enzymes [23, 24].

2.3 | Catalytic Properties of the Mutant CYP199A4 Enzymes

Having a range of potentially interesting CYP199A4 mutants at hand, we decided to evaluate their catalytic properties in the oxidative demethylation of *para*-methoxy benzoic acid [10].

In these experiments especially the double mutant CYP199A4$^{F182R/T252E}$ stood out in terms of product formation (Figure 4). To our surprise, however, the previously reported single mutant CYP199A4^{T252E} yielded less product than the wild-type enzyme, which is in stark contrast to the results previously

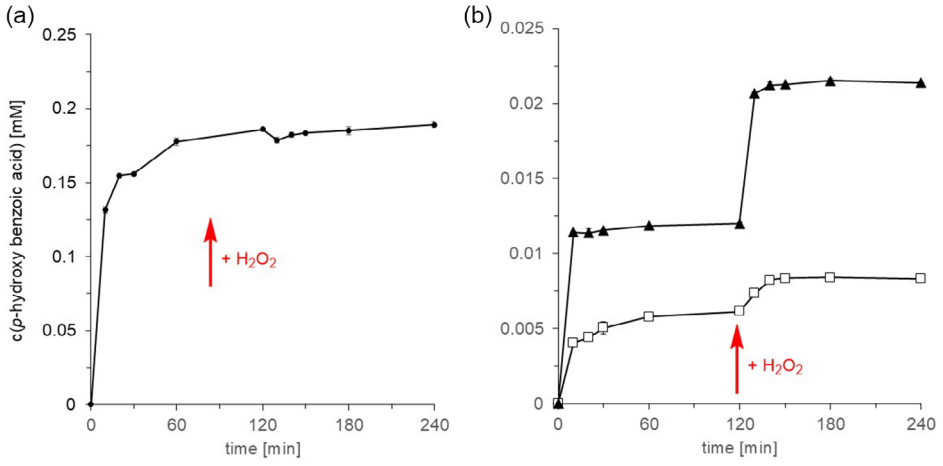

FIGURE 5 | Time courses of purified CYP199A4 (variants) catalyzed O-demethylation reactions using H_2O_2 as cosubstrate. (A): using CYP199A4$^{T252E/F182R}$ (•), (B) using CYP199A4^{wt} (□) or CYP199A4^{T252E} (▲). Reaction conditions: 50 mM KPi buffer (1 vol% EtOH) pH 7.5, total volume 2 mL (in horizontal shaker, 600 rpm), $T = 30°C$, $t = 3.5$ h; c(CYP199A4) = 6 µM, c(4-methoxybenzoic acid) = 1 mM, $c(H_2O_2)_{final}$ = 20 mM (added in two steps a $t = 0$ and 120 min). Values represent the average of duplicates. Note the different scales used for CYP199A4$^{F182R/T252E}$ (A) and CYP199A4^{wt} and CYP199A4^{T252E} (B).

TABLE 1 | Catalase activity of the CYP199A4 variants.[a]

	Catalase activity, μmol O_2 min^{-1} $mg^{-1}_{CYP199A4}$		
	CYP199A4^{wt}	**CYP199A4^{T252E}**	**CYP199A4$^{F182R/T252E}$**
No additives	3.9	2.9	0.15
+ Ethanol[a]	2.0	1.7	0.02
+ *p*-Methoxy benzoic acid + ethanol[b]	1.8	1.3	—[c]

General conditions: 50 mM KPi buffer pH 7.5 at room temperature, c(CYP199A4) = 3 μM, $c(H_2O_2)$ = 1 mM.
[a]c(4-methoxybenzoic acid) = 1 mM.
[b]c(4-methoxybenzoic acid) = 1 mM, c(EtOH) = 5% (v/v). The catalase activities were determined via the O_2 accumulation in the anaerobic reaction mixture upon H_2O_2 addition (measured with a Clark electrode).
[c]not detected. Contamination with endogeneous *E. coli* catalase cannot be fully ruled out. However, all variants were expressed and purified using the same protocol, and the higher expression of WT and T252E meant that markedly smaller volumes of enzyme fraction were required to reach 3 μM in the Clark electrode assay (27 and 86 μL) than for F182R/T252E (236 μL), which would be expected to reduce any impurity-driven oxygen evolution. Thus, the observed trend is not readily explained solely by variable impurity carryover.

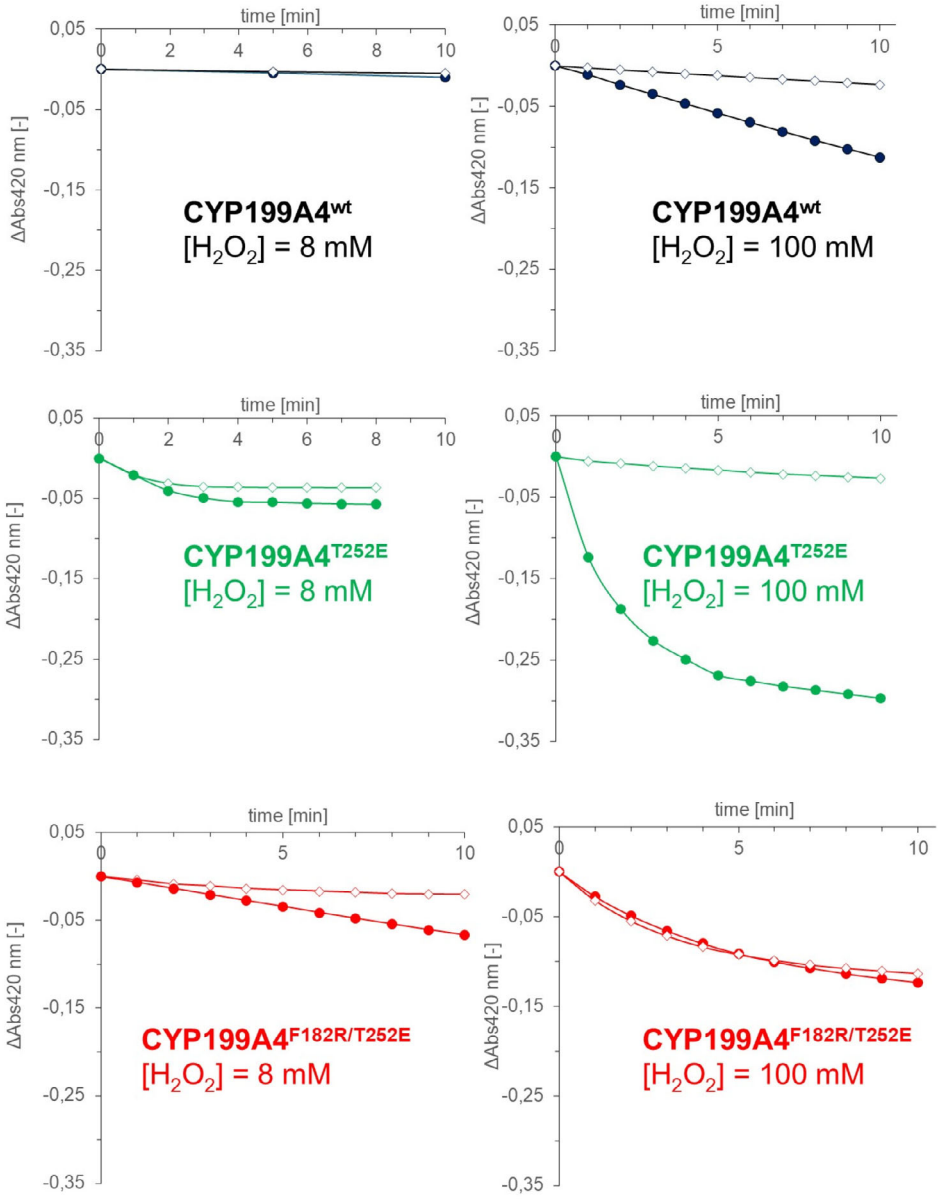

FIGURE 6 | Heme bleaching experiments with **CYP199A4^{wt}**, **CYP199A4^{T252E}**, and **CYP199A4$^{F182R/T252E}$** in the absence (●●●) and presence (◇◇◇) of and oxidizable substrate. Conditions: 50 mM KPi pH 7.5 containing 5% (v/v) EtOH, c(CYP199A4) = 3 μM, c(*p*-methoxy benzoic acid) = 0 or 1 mM, $c(H_2O_2)$ = 8 or 100 mM, RT.

reported (vide infra). Possibly, endogenous *E. coli* catalase influenced the outcome of the preliminary screening, but said effect would be equal between samples, thus yielding a proper comparison. We purified wild-type enzyme, the single mutant (T252E), and our double mutant (T252E/F182R) to accurately investigate the time-course of the H_2O_2-driven O-demethylation reaction (Figure 5).

Notably, the initial rate (and final product concentration) achieved with CYP199A4$^{F182R/T252E}$ was about one order of magnitude higher than with CYP199A4^{wt} and CYP199A4^{T252E}. The estimated specific activities for the three variants were 1.5, 4.2, and 48.3 mU mg^{-1} for the wild-type, CYP199A4^{T252E} and CYP199A4$^{F182R/T252E}$, respectively. These values are likely to be substantially underestimated, as most of the transformation had already occurred before the first measurement at 10 min. All transformations ceased within a maximum of 60 min. In the case of CYP199A4^{wt} and CYP199A4^{T252E}, further addition of H_2O_2 to the reaction mixtures led to additional product formation, indicating a pronounced catalase activity in these two variants. In contrast, the addition of further H_2O_2 did not resume product formation in the case of CYP199A4$^{F182R/T252E}$, suggesting that this enzyme variant had been irreversibly inactivated, presumably due to H_2O_2 exposure. A possible thermal inactivation of CYP199A4$^{F182R/T252E}$ was excluded (Figure S6).

We therefore tested the catalase activity of the three CYP199A4 variants using a Clark electrode setup (Table 1). It is important to highlight that the enzyme and H_2O_2 concentrations used for the demethylation experiment differ from the ones used for the catalase experiment. This is due to the high sensitivity of the Clark electrode, thus making it unfeasible to obtain accurate estimations under the same reaction conditions. Indeed, the catalase activity of wild type enzyme and single mutant were more than 10 times higher than of CYP199A4$^{F182R/T252E}$. Interestingly, substrate addition reduced the catalase activity by only approx. 40%–50% in case of CYP199A4^{wt} and CYP199A4^{T252E} whereas it reduced the catalase activity of CYP199A4$^{F182R/T252E}$ by almost 90%.

This observation also partially explains the higher initial activity of CYP199A4$^{F182R/T252E}$ compared to CYP199A4^{wt} and CYP199A4^{T252E} (Figure 4 and 5). Their catalase activity is much higher than the catalase activity of CYP199A4$^{F182R/T252E}$. Furthermore, their catalase activity is only reduced by half in the presence of substrate. Overall, the reactions catalyzed by CYP199A4^{wt} and CYP199A4^{T252E} were strongly constrained by H_2O_2 availability, indicating that peroxide supply is a primary rate- and/or extent-limiting factor under the conditions tested.

To gain a deeper understanding, we also investigated the H_2O_2-dependent bleaching of the catalytic heme moiety in the presence of H_2O_2 (Figure 6). Interestingly, the wild-type enzyme turned out to be the least H_2O_2-sensitive CYP199A4 variant whereas CYP199A4^{T252E} was inactivated the fastest by H_2O_2. In the presence of lower H_2O_2 concentrations (8 mM,), CYP199A4^{wt} showed almost negligible inactivation rate of 0.001% min^{-1}, whereas the single mutant exhibited a significantly (approx. 30-times) higher initial inactivation rate. Due to its inherent high catalase activity (Table 1), however, all initial H_2O_2 was dismutated within 2 min thereby ceasing heme bleaching. The inactivation rate of the double mutant (0.016 min^{-1}) was between wild type and the single mutant. However, due to the low catalase activity, heme bleaching continued linearly for at least 20 min. In the presence of high concentrations of H_2O_2 (Figure 6) heme bleaching was accelerated approximately threefold for all variants. Interestingly, in the case of CYP199A4^{wt} and CYP199A4^{T252E,} the presence of substrate dramatically reduced heme bleaching while in the case of CYP199A4$^{F182R/T252E}$, it had almost no effect on the heme bleaching rate.

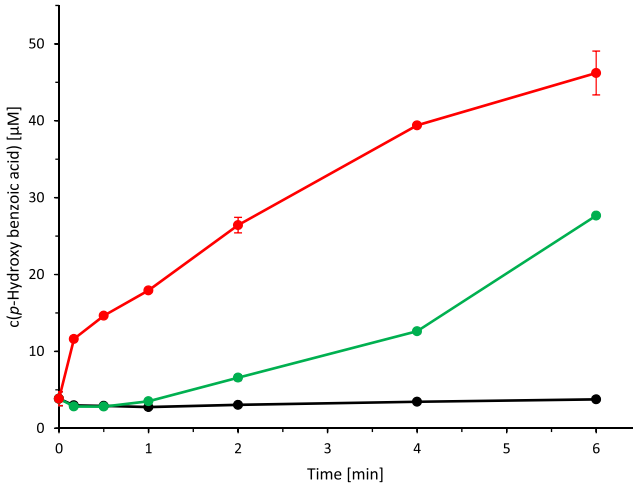

FIGURE 7 | Time courses of **CYP199A4^{wt}** (black), **CYP199A4^{T252E}** (green), and **CYP199A4$^{F182R/T252E}$** (red). Reaction conditions: 50 mM KPi buffer (1 vol% EtOH), pH 7.5, total volume 2 mL (in horizontal shaker, 600 rpm), $T = 30°C$, $t = 6$ h; c(CYP199A4) = 6 µM, c(4-methoxybenzoic acid) = 1 mM, $c(H_2O_2)_{final} = 0.6$ mM (feeding of 0.1 mM h^{-1}). Values represent the average of duplicates.

From these experiments, we concluded that the reaction yield was severely limited by the bleaching effect of H_2O_2 on the CYP199A4 variants. More specifically, complete degradation of CYP199A4$^{F182R/T252E}$ occurred within the first 30 min when H_2O_2 was supplied at 10 mM h^{-1} (Figure 5). We therefore investigated the effect of reducing the H_2O_2 feed rate to 0.1 mM h^{-1} (Figure 7). Under these conditions, most of the H_2O_2 supplied to CYP199A4^{wt} and CYP199A4^{T252E} was rapidly disproportionated due to their catalase activity. By contrast, CYP199A4$^{F182R/T252E}$ was able to drive the reaction almost immediately and continued to do so for several hours, demonstrating that bleaching can be controlled by carefully tuning the rate of H_2O_2 addition.

It is also noteworthy that with CYP199A4$^{F182R/T252E}$, the initial rate of *p*-hydroxybenzoate formation was 0.07 mM h^{-1} (corresponding to 70% utilization of the supplied H_2O_2), but this decreased tenfold (to 0.007 mM h^{-1}, i.e. 7%) over the following 3 h. While ethanol oxidation is a likely contributor to this decline, we currently lack a plausible explanation for why it becomes significant only after a few enzyme turnovers. A possible starting point for rationalization may be substrate-binding competition between ethanol and *p*-methoxybenzoate. It is also worth mentioning that in case of CYP199A4^{T252E} the product accumulation seemed to increase, for which we have no plausible explanation yet.

3 | Conclusion

The aim of this study was to improve the peroxygenase activity of CYP199A4^{T252E} by introducing a second base to mimic the architecture of classical peroxygenase. We hypothesized that

the charge delocalization may accelerate the deprotonation/reprotonation of the initial heme-Fe^{3+}-H_2O_2 adduct and facilitate formation of CpdI. The significantly higher initial activity of $CYP199A4^{F182R/T252E}$ over the wt-enzyme and the parent $CYP199A4^{T252E}$ seem to confirm this assumption. $CYP199A4^{F182R/T252E}$, however, also exhibited a significantly decreased stability towards H_2O_2, which we attribute to the decreased catalase activity.

The broadly accepted hypothesis for heme-enzyme inactivation in the presence of excess H_2O_2 assumes a catalase malfunction reaction. In the catalase mode, in which CpdI in the absence of an organic reductant, reacts with another H_2O_2, yielding CpdII and a peroxyl radical ($HO_2^{\bullet}$). To complete the catalase cycle, $HO_2^{\bullet}$ needs to undergo an electron transfer to CpdII and deprotonation to yield O_2 and Cpd0. If, however, this reaction is slow, $HO_2^{\bullet}$ can leave, making space for yet another H_2O_2 equivalent, eventually forming CpdIII (a ferric superoxide adduct, Fe^{III}–$HO_2^{-\bullet}$) initiating Haber-Weiss-type formation of free reactive oxygen species eventually responsible for oxidative heme degradation.

Acknowledgments

Funded by the European Union (ERC, PeroxyZyme, No 101054658). Views and opinions expressed are however those of the authors only and do not necessarily reflect those of the European Union or the European Research Council. Neither the European Union nor the granting authority can be held responsible for them.

Funding

This study was supported by HORIZON EUROPE Framework Programme (ERC, PeroxyZyme, No 101054658).

Conflicts of Interest

The authors declare no conflicts of interest.

Data Availability Statement

The data that support the findings of this study are available from the corresponding author upon reasonable request.

References

1. V. B. Urlacher and S. Eiben, "Cytochrome P450 Monooxygenases: Perspectives for Synthetic Application," *Trends in Biotechnology* 24 (2006): 324–330.

2. M. R. Juchau, "Substrate Specificities and Functions of the P450 Cytochromes," *Life Sciences* 47 (1990): 2385–2394.

3. D. Holtmann and F. Hollmann, "The Oxygen Dilemma: A Severe Challenge for the Application of Monooxygenases?," *ChemBioChem* 17 (2016): 1391–1398.

4. D. F. V. Lewis, and J. M. Pratt, "The P450 Catalytic Cycle and Oxygenation Mechanism," *Drug Metabolism Reviews* 30 (2008): 739–786.

5. R. A. Kahn, F. Durst, J. T. Romeo, et al., *in Recent Advances in Phytochemistry*. 34, eds.: J. T. Romeo, R. Ibrahim, L. Varin, and V. De Luca, (Elsevier, 2000), 151–189.

6. O. Shoji and Y. Watanabe, "Peroxygenase Reactions Catalyzed by Cytochromes P450," *Journal of Biological Inorganic Chemistry* 19 (2014): 529–539.

7. M. N. Podgorski and S. G. Bell, "Comparing and Combining Alternative Strategies for Enhancing Cytochrome P450 Peroxygenase Activity," *ACS Catalysis* 15 (2025): 5191–5210.

8. M. N. Podgorski, J. Akter, L. R. Churchman, J. B. Bruning, J. J. De Voss, and S. G. Bell, "Engineering Peroxygenase Activity into Cytochrome P450 Monooxygenases through Modification of the Oxygen Binding Region," *ACS Catalysis* (2024): 7426–7443.

9. M. N. Podgorski, J. H. Z. Lee, J. S. Harbort, et al., "Characterisation of the Heme Aqua-Ligand Coordination Environment in an Engineered Peroxygenase Cytochrome P450 Variant," *Journal of Inorganic Biochemistry* 249 (2023): 112391.

10. M. N. Podgorski, J. S. Harbort, J. H. Z. Lee, et al., "An Altered Heme Environment in an Engineered Cytochrome P450 Enzyme Enables the Switch from Monooxygenase to Peroxygenase Activity," *ACS Catalysis* 12 (2022): 1614–1625.

11. S. Fan and Z. Cong, "Emerging Strategies for Modifying Cytochrome P450 Monooxygenases into Peroxizymes," *Accounts of Chemical Research* 57 (2024): 613–624.

12. P. Zhao, F. Kong, Y. Jiang, X. Qin, X. Tian, and Z. Cong, "Enabling Peroxygenase Activity in Cytochrome P450 Monooxygenases by Engineering Hydrogen Peroxide Tunnels," *Journal of the American Chemical Society* 145 (2023): 5506–5511.

13. J. Xu, C. Wang, and Z. Cong, "Strategies for Substrate-Regulated P450 Catalysis: From Substrate Engineering to Co-catalysis," *Chemistry – A European Journal* 25 (2019): 6853–6863.

14. N. Ma, Z. Chen, J. Chen, et al., "Dual-Functional Small Molecules for Generating an Efficient Cytochrome P450BM3 Peroxygenase," *Angewandte Chemie International Edition* 57 (2018): 7628–7633.

15. K. Piontek, R. Ullrich, C. Liers, K. Diederichs, D. A. Plattner, and M. Hofrichter, "Crystallization of a 45 kDa Peroxygenase/Peroxidase from the Mushroom *Agrocybe Aegerita* and Structure Determination by SAD Utilizing Only the Haem Iron," *Acta Crystallographica Section F: Structural Biology and Crystallization Communications* 66 (2010): 693–698.

16. R. Ullrich, J. Nüske, K. Scheibner, J. Spantzel, and M. Hofrichter, "Novel Haloperoxidase from the Agaric Basidiomycete *Agrocybe Aegerita* Oxidizes Aryl Alcohols and Aldehydes," *Applied and Environmental Microbiology* 70 (2004): 4575–4581.

17. A. Beltrán-Nogal, I. Sánchez-Moreno, D. Méndez-Sánchez, P. Gómez de Santos, F. Hollmann, and M. Alcalde, "Surfing the Wave of Oxyfunctionalization Chemistry by Engineering Fungal Unspecific Peroxygenases," *Current Opinion in Structural Biology* 73 (2022): 102342.

18. P. Molina-Espeja, S. Ma, D. M. Mate, R. Ludwig, and M. Alcalde, "Tandem-Yeast Expression System for Engineering and Producing Unspecific Peroxygenase," *Enzyme and Microbial Technology* 73-74 (2015): 29–33.

19. P. Molina-Espeja, E. Garcia-Ruiz, D. Gonzalez-Perez, R. Ullrich, M. Hofrichter, and M. Alcalde, "Directed Evolution of Unspecific Peroxygenase from Agrocybe Aegerita," *Applied and Environmental Microbiology* 80 (2014): 3496–3507.

20. H. Land and M. S. Humble, In *Protein Engineering: Methods and Protocols*. eds.: U. T. Bornscheuer and M. Höhne, (Springer New York, 2018), 43–67.

21. D. Linde, E. Santillana, E. Fernández-Fueyo, et al., "Structural Characterization of Two Short Unspecific Peroxygenases: Two Different Dimeric Arrangements," *Antioxidants* 11 (2022): 891.

22. P. J. Mak and I. G. Denisov, "Spectroscopic Studies of the Cytochrome P450 Reaction Mechanisms," *Biochimica et Biophysica Acta (BBA) - Proteins and Proteomics* 1866 (2018): 178–204.

23. H. Matsumura, M. Wakatabi, S. Omi, et al., "Modulation of Redox Potential and Alteration in Reactivity via the Peroxide Shunt Pathway by Mutation of Cytochrome P450 around the Proximal Heme Ligand," *Biochemistry* 47 (2008): 4834–4842.

24. Y. Shibata, H. Sato, I. Sagami, and T. Shimizu, "Interaction of Angeli's Salt with Cytochrome P450 1A2 Distal Mutants: an Optical Absorption Spectral Study," *Biochimica et Biophysica Acta (BBA) - Protein Structure and Molecular Enzymology* 1343 (1997): 67–75.

25. M. Kayikci, A. J. Venkatakrishnan, J. Scott-Brown, C. N. J. Ravarani, T. Flock, and M. M. Babu, "Visualization and Analysis of Non-Covalent Contacts Using the Protein Contacts Atlas," *Nature Structural & Molecular Biology* 25 (2018): 185–194.

26. H. Land, M. S. Humble, "YASARA: A Tool to Obtain Structral Guidance in Biocatalytic Investigations," *Methods in Molecular Biology* 1685 (2018): 43–67.

27. T. Omura, R. R. Sato, "The Carbon Monoxide-Binding Pigment of Liver Microsomes," *The Journal of Biological Chemistry* 239 (1964): 2370–2378.

Supporting Information

Additional supporting information can be found online in the Supporting Information section. The authors have cited additional references within the Supporting Information [25–27]. **Supporting Fig. S1:** Residues with more interactions with the heme cofactor into the structure of CYP199A4^{T252E}. The size of the circles is proportional to the number of interactions and inner and outer rings represent immediate and secondary atom contacts. Different colors represent different secondary structures. **Supporting Fig. S2:** YASARA minimal energy simulation of the catalytic pocket of CYP199A4^{T252E} before (A) and after (B) the F182R mutation. Heme is shown in red, 252E is shown in dark red, substrate is shown in cyan and 182 residue is shown in yellow. **Supporting Fig. S3:** SDS-PAGE from crude extract of produced CYP199A4^{WT}, CYP199A4^{T252E} and CYP199A4^{T252E} variants in *E.coli* 43(DE3). 10 µl of Precision Plus Protein Unstained Standard (Biorad) was used as ladder and protein loading was 1 mg/ml. **Supporting Fig. S4:** UV analysis at 280 nm during HisTag purification of CYP199A4^{T252E} variants. The blue and orange line correspond to the absorbance at 280 and 420 nm respectively. **Supporting Fig. S5:** SDS-PAGE and CO-diff spectra of purified CYP199A4 variants. Both A and B are fractions from the same purification but with different dilutions. This was done due to the size of the volume of the pure fraction. **Supporting Fig. S6:** CO-difference spectra of pure and incubated CYP199A4$^{F182R/T252E}$. **Supporting Fig. S7:** Product formation of CYP199A4$^{F182R/T252E}$ with different cosolvents. Reaction conditions: 50 mM KPi buffer (5 vol% cosolvent) pH 7.5, total volume 1 ml (in horizontal shaker, 600 rpm), T = 30°C, t = 3.5 hr; c(CYP199A4) = 6 µM, c (4-methoxybenzoic acid) = 1 mM, $c(H_2O_2)_{final}$ = 10 mM. Values represent the average of duplicates. **Supporting Fig. S8:** HPLC analysis of screening of CYP194A4 variants for peroxygenase activity. Reaction conditions: 50 mM KPi buffer (2 vol% ACN) pH 7.5, total volume 0.5 ml (in horizontal shaker, 600 rpm), T = 30°C, t = 3.5 hr; c(CYP199A4) = 2.5 µM enzyme (crude extract) c (4-methoxybenzoic acid) = 1 mM, $c(H_2O_2)_{final}$ = 25 mM (added in two steps). Reverse phase HPLC with 20-95% gradient of ACN in water. **Supporting Table S1**: List of designed primers for the site directed mutagenesis of CYP199A4^{T252E} candidates.